Molecular Mechanism of H_2O Diffusion into Polyimides: A Model Based on Dual Mobility with Instantaneous Local Nonlinear Equilibrium

Giuseppe Mensitieri,*,† Marino Lavorgna,‡ Domenico Larobina,‡ Giuseppe Scherillo,† Giuseppe Ragosta,§ and Pellegrino Musto§

Department of Materials and Production Engineering, University of Naples Federico II, P.le Tecchio 80, 80125, Naples, Italy; Institute of Composite and Biomedical Materials, National Research Council of Italy, P.le Tecchio 80, 80125, Naples, Italy; and Institute of Chemistry and Technology of Polymers, National Research Council of Italy, Via Campi Flegrei, 34, 80078, Pozzuoli, Naples, Italy

Received February 27, 2008; Revised Manuscript Received April 18, 2008

ABSTRACT: The mass transport mechanism of water into polyimide films has been analyzed and modeled on the basis of the relevant findings of an in situ FTIR spectroscopic analysis, performed previously, which (i) identified a molecular mechanism of diffusion based on two water species, i.e., H_2O molecules interacting with the carbonyl groups of the polyimide and self-associated water, and (ii) evidenced the establishment of an instantaneous nonlinear equilibrium between these species. To model water transport, it has been assumed that concurrent diffusion occurs of two species, i.e., single water molecules and water dimers, which display different mobilities. A nonlinear instantaneous equilibrium between the local concentrations of these two species has been imposed. This equilibrium relationship has been derived on the basis of a two-layer BET (Brunauer, Emmett, and Teller) theory for the water sorption isotherm. The proposed approach is able to give a good qualitative and quantitative interpretation of both sorption equilibrium and of sorption/desorption kinetics data collected for each of the two water species identified by FTIR spectroscopy.

Introduction

Polyimides are well-known for their outstanding properties in terms of thermal-oxidative stability, mechanical performances, high glass transition temperature (T_g), and good resistance to solvents.[1−4] These properties make them attractive for microelectronic and opto-electronic applications and as membranes for separation technologies.[5−8]

With respect to the sorption thermodynamics and mass transport behavior of low molecular weight compounds, transport of water has obvious technological implications, especially in microelectronic applications where absorbed moisture may cause reliability problems such as increase in dielectric constant, metal corrosion of devices, loss of adhesion, and mechanical failures.[9−11] Water diffusion in polyimides has been shown to be a complex process[10−13] whose mechanism is still incompletely understood at a molecular level. It has been shown that both the amount of water sorbed at equilibrium and the diffusivity depend strongly on the structure of the polyimide chain, which confirms the importance taken by the "interaction effect" and implies that any modeling attempt must be firmly grounded on a molecular level description of the whole system. Among the various issues to be addressed, the principal ones are (i) the type of molecular interactions, (ii) the nature and the number of the interacting species (polymer−pentrant interactions and/or penetrant self-interactions), and (iii) a quantitative estimation of the various species present in the system both at equilibrium and during their dynamic evolution.

In a previous contribution[14] the transport of H_2O in pyromellitic dianhydride−oxydianiline (PMDA−ODA) polyimide films was investigated by means of time-resolved FTIR spectroscopy, making use of several methods of vibrational data analysis. This study supplied a wealth of information about the interactional issues and sorption/desorption kinetics of the water/polyimide system. The present work is aimed at developing a macroscopic model for sorption thermodynamics and water transport grounded on the relevant results of the FTIR analysis. The modeling is based on the physical picture of an instantaneous local nonlinear equilibrium between two distinct water species evolving with different kinetics. The model captures effectively some salient qualitative features of the equilibrium and dynamic behavior of the system, also supplying a semiquantitative interpretation of the observed phenomena.

Experimental Section

Materials. The polyimide precursor used in this study was a polyamic acid, Pyre-ML RK 692 from I.S.T (Indian Orchard, MA). It was obtained by condensation of PMDA-ODA and had a molecular weights $\bar{M}_w = 1.0 \times 10^5$ and $\bar{M}_n = 4.6 \times 10^4$. It was supplied as a 12 wt % solution in a mixture of *N*-methyl-2-pyrrolidone (NMP) and xylene (weight ratio 80/20).

Preparation of the Polyimide Films. Two kinds of films have been used in the present investigation: (a) 20−30 μm thick castings and (b) 3.2−1.0 μm spin-coated films. The former were employed for the evaluation of sorption/desorption kinetics, while the latter were used to evaluate sorption isotherms. The preparation procedures and the curing protocol are detailed in ref 14.

Techniques. A vacuum-tight FTIR cell was used to record the FTIR transmission spectra of the polymer films exposed to water vapor at constant pressure. The cell was connected through service lines to a water reservoir, a vacuum pump, and pressure transducers. Full details of the experimental setup are reported in refs 15 and 16.

Sorption−desorption tests were performed at 30 °C and at relative pressures, p/p_0, varying from 0.1 to 0.80 (where p is the experimental pressure and p_0 is the saturation pressure of water vapor at 30 °C, corresponding to 31.8 Torr). The relative pressure was assumed to be equal to the water activity, a_w, in view of the low value of p_0. Full details on the FTIR data analysis are reported in ref 14.

* Corresponding author.
† University of Naples Federico II.
‡ Institute of Composite and Biomedical Materials, National Research Council of Italy.
§ Institute of Chemistry and Technology of Polymers, National Research Council of Italy.

10.1021/ma8004422 CCC: $40.75
Published on Web 06/11/2008

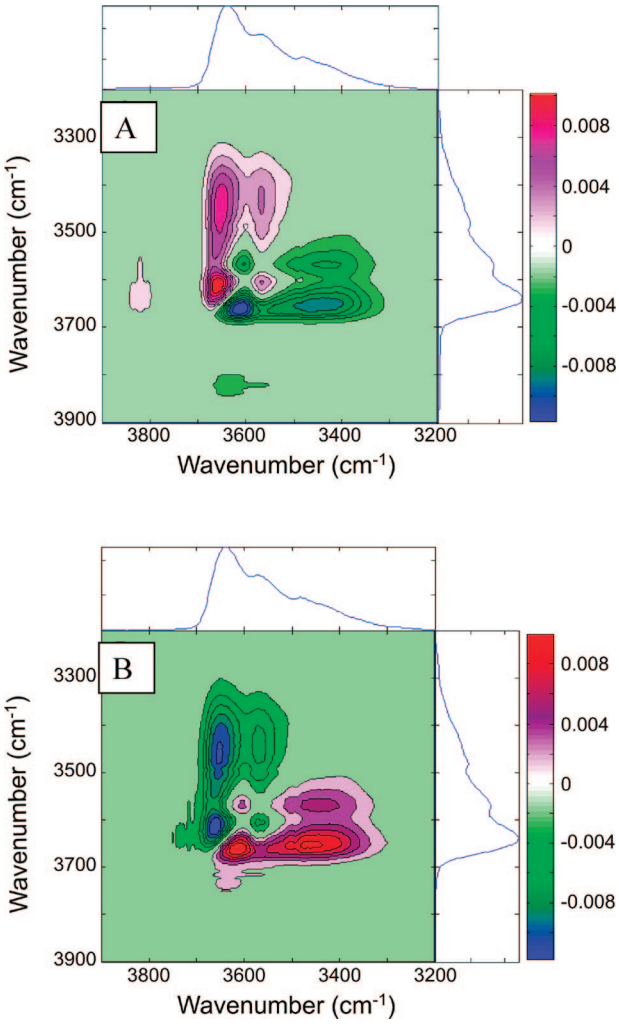

Figure 1. 2D-FTIR correlation spectra obtained by the analysis of the spectra collected during sorption/desorption experiments on the polyimide film: (A) asynchronous spectrum for the sorption test at $a_w = 0.6$; (B) asynchronous spectrum for the desorption test at $a_w = 0.6$. $T = 30$ °C.

Results and Discussion

FTIR Spectroscopy Results. In this section we provide an overview of the spectroscopic results[14] more relevant to the development of a model for water sorption thermodynamics and kinetics in PMDA-ODA. Time-resolved FTIR spectra were collected in situ during water vapor sorption/desorption tests under controlled temperature and relative humidity conditions. Among the different approaches employed for the interpretation of these data, 2D-FTIR correlation spectroscopy[17] was found particularly rewarding. This technique is capable of improving the resolution by spreading the data on a second frequency axis and, at the same time, is able of providing information about the kinetics of the evolving system. In Figure 1A is reported the asynchronous correlation spectrum relative to a sorption test at $a_w = 0.6$.

It is worth recalling that a peak in the asynchronous spectrum at $[\nu_1, \nu_2]$ corresponds to two IR signals changing at different rates. Conversely, if two signals change at the same rate, they will produce zero intensity in the spectrum, thus providing the characteristic resolution enhancement and the specificity of this pattern. Also relevant is the sign of the correlation peaks, which yields information about the sequence of changes of the two IR signals involved, according to the so-called Noda's rules.[17,18] The interpretation of the overall pattern depicted in Figure 1A points[14] to the presence of two couples of signals at 3660−3570 and 3616−3456 cm^{-1}. The two components of each couple change at the same rate, but the two couples evolve with a different dynamics.

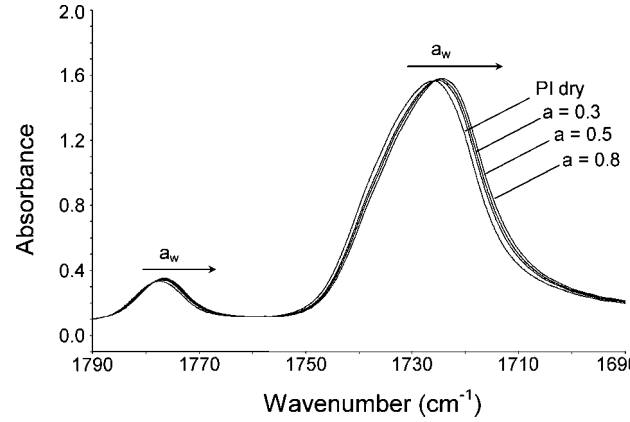

Figure 2. Carbonyl region of a polyimide spectrum (thickness 2.4 μm) in the dry state and equilibrated at different water vapor activities. $T = 30$ °C.

The analysis of the carbonyl range (1800−1680 cm^{-1}) allowed us to identify the interaction sites along the polymer backbone. A shift of both the in-phase and out-of-phase carbonyl stretching modes toward lower wavenumbers was observed in the presence of sorbed water. This effect is demonstrated in Figure 2, where it is also evident that the extent of the shift is an increasing function of the water absorbed at equilibrium. Desorption experiments demonstrated that the effect is fully reversible. The above evidence confirmed that the imide carbonyls represent the proton acceptors to which water molecules are bound.

The whole of the spectroscopic results was interpreted[14] by assuming the occurrence of two distinct water species, each producing two peaks. In particular, the 3660 and 3570 cm^{-1} peaks were assigned respectively to the out-of-phase and in-phase stretching modes of H_2O molecules bound to imide carbonyls via a H-bonding interaction (referred to, in the following, as "bound water", *b*). The two peaks at 3616 and 3470 cm^{-1} have been related to self-associated water in the form of (predominantly) water dimers (referred to, in the following, as "self-associated water", *sa*). In particular, the feature at 3616 cm^{-1} has been assigned to a ν(O−H) localized primarily on the noninteracting O−H bond, whereas the 3470 cm^{-1} band was ascribed to the stretching mode of the interacting O−H bond. It should be pointed here that, on the basis of the spectroscopic analysis, there is no conclusive evidence that the self-associated water is strictly a dimer. However, taking into account the very low concentration of self-associated water, it is highly probable that dimers represent the dominant self-associated species. The proposed structure of the polyimide/H_2O aggregate is depicted in Scheme 1.

In the frame of the model to be developed, the population of water molecules interacting with the polymer backbone can be described in terms of two components: (a) R_1, i.e., a single water molecule interacting with an imide group via H-bonding interaction (associated with 3660−3570 cm^{-1} peaks), (b) R_2 species, i.e., water molecules dimers made of a water molecule bound to an imide group (producing the peaks at 3660−3570 cm^{-1}) and a self-associated water molecule (giving rise to the peaks at 3616−3470 cm^{-1}). Straightforward relationships can be written relating the concentration of bound and self-associated water molecules (experimentally determined spectroscopically) to the concentration of R_1 and R_2 species used in the modeling. Further discussion on this point is deferred to the section dealing with mass transport analysis. With R_0, we indicate the unoccupied imide group on the polymer backbone.

Scheme 1

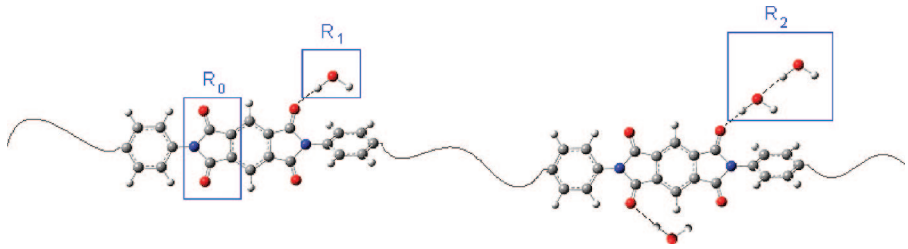

Further information can be gathered by comparing the asynchronous contour maps relative to the sorption and desorption experiments. It is noted that the two patterns are coincident but with the sign reversed (compare parts A and B of Figure 1). This indicates that the species sorbed at a faster rate ($[H_2O]_b$) are released at a slower rate with respect to the dimeric species ($[H_2O]_{sa}$) during desorption.

Another approach to investigate the dynamics of the system is represented by the direct comparison of the stretching and bending absorbance areas, as measured during the different kinetic tests. This approach can be useful to discriminate between linear and nonlinear equilibria among the diffusing species and can provide insight into the relative diffusion rates. An absorbance−absorbance plot of this kind, relative to all investigated activities, is shown in Figure 3.

The principles upon which the method relies can be outlined as follows: The ratio between the stretching and bending absorbances is related to the concentration of the two water species through the following equation:[15,19,20]

$$\frac{A_\nu^{TOT}}{A_\delta^{TOT}} = \frac{\varepsilon_{3660}C_b + \varepsilon_{3616}C_{sa} + \varepsilon_{3570}C_b + \varepsilon_{3456}C_{sa}}{\varepsilon_b C_b + \varepsilon_{sa} C_{sa}} \quad (1)$$

where $A_\nu^{TOT}$and A_δ^{TOT} are the total absorbance areas in the stretching (ν) and bending (δ) regions, respectively, C_i's represent molar concentrations, and ε_i's are the molar absorptivities. Numerical subscripts indicate peak frequencies; b and sa subscripts have the usual meaning.

It is well-known from the literature that the bending modes are far less sensitive than the stretching modes to H-bonding interactions in terms of absolute intensity.[21,22] This has been confirmed for the present system by ab initio normal coordinate analysis calculations.[14] Accordingly, we may assume $\varepsilon_b \cong \varepsilon_{sa} = \varepsilon_\delta$, and rearranging eq 1 in terms of molar fraction x_i

$$\frac{A_\nu^{TOT}}{A_\delta^{TOT}} = \frac{x_b(\varepsilon_{3660} + \varepsilon_{3570}) + x_{sa}(\varepsilon_{3616} + \varepsilon_{3456})}{\varepsilon_\delta} \quad (2)$$

where

$$x_b = \frac{C_b}{C_b + C_{sa}} \quad (3)$$

$$x_{sa} = \frac{C_{sa}}{C_b + C_{sa}} \quad (4)$$

Thus, the slope, α, of the A_ν^{TOT} vs A_δ^{TOT} diagram, using the mass balance equation, may be expressed as

$$\alpha = A + (B - A)x_{sa} \quad (5)$$

where $A = (\varepsilon_{3660} + \varepsilon_{3570})/\varepsilon_\delta$ and $B = (\varepsilon_{3616} + \varepsilon_{3456})/\varepsilon_\delta$.

From eq 2 it follows that if the molar fractions remain constant during the sorption process (instantaneous, linear equilibrium between the two water species), in the absorbance−absorbance diagram the experimental data can be accommodated on a linear master curve passing through the origin. Conversely, whenever the molar fractions change (instantaneous, nonlinear equilibrium), a significant departure from linearity is observed. In the present case the data can be suitably accommodated on a single master curve through the origin, but an upward concavity is apparent for abscissa values exceeding 5 absorbance units, which corresponds to the data gathered at water vapor activities above 0.3. In eq 2, the term ($\varepsilon_{3616} + \varepsilon_{3456}$) is largely prevailing over the term ($\varepsilon_{3660} + \varepsilon_{3570}$) owing to the fact that the molar absorptivity of ν_{OH} vibrations increases substantially (up to 10 times) with the strength of the H-bonding interaction, and, consequently, with the lowering of the peak frequency.[21,22] Therefore, in eq 5, $B \gg A$ and α increases when the molar fraction of self-associated water increases. Hence, the upward concavity of the plot of Figure 3 implies that, in the later stages of the sorption process, the overall population of sorbed water is enriched in terms of dimeric species (R_2), indicating that H_2O molecules bound to carbonyls reach saturation before the dimeric species. This, in turn, points to a faster initial rate of diffusion of the former species, in agreement with the results of 2D-FTIR spectroscopy discussed earlier.

The spectrum of sorbed water can be isolated by means of spectral subtraction analysis, as described in detail in ref 14. A typical ν_{OH} profile relative to the equilibrium water uptake at $a_w = 0.4$ is reported in Figure 4 along with the results of a least-squares curve-fitting (LSCF) analysis.

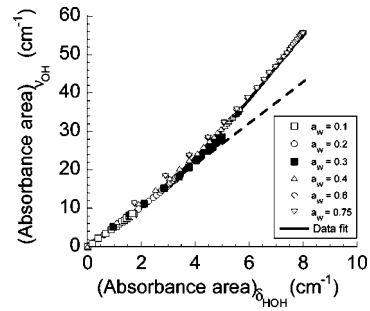

Figure 3. Absorbance area of the ν_{OH} water band as a function of the absorbance area of the δ_{HOH} water band for sorption experiments performed at the different activities. $T = 30$ °C.

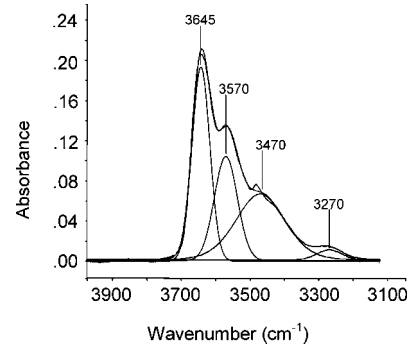

Figure 4. Least-squares curve-fitting analysis of the spectrum representative of water sorbed at equilibrium ($a_w = 0.4$) in the polyimide film. The figure displays the experimental profile, the best-fitting curve, and the four resolved components. $T = 30$ °C.

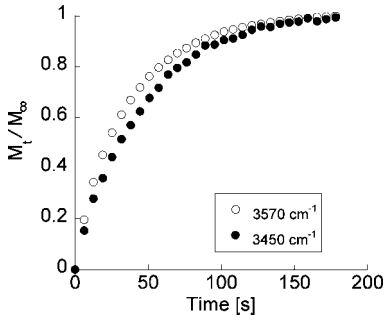

Figure 5. Sorbed mass normalized for the equilibrium mass uptake as a function of time for the sorption test at $a_w = 0.4$: (○) water bound to imide carbonyls; (●) self-associated water. $T = 30$ °C.

A detailed assignment of the various components is reported in ref 14; here we focus on the peaks at 3570 and 3470 cm^{-1} representative respectively of the out-of-phase ν_{OH} mode of H_2O bound to carbonyls and the ν_{OH} mode of self-interacting water. The LSCF analysis of the time-resolved data allows us to monitor quantitatively the evolution of the two water species in terms of normalized mass. This is reported in Figure 5, where sorbed mass at time t, normalized for the equilibrium mass uptake (M_t/M_∞, which corresponds to A_t/A_∞), is plotted as a function of time for the test at $a_w = 0.4$. Here again the faster sorption rate of the H_2O species bound to carbonyls is evident.

Modeling of Water Sorption Thermodynamics and Mass Transport. *Sorption Isotherms.* Modeling of equilibrium sorption behavior of low molecular weight compounds in a glassy polymer should take into account the nonequilibrium nature of the polymer. To this aim, a relatively recent approach has been proposed in the literature,[23] based on the thermodynamics of internal state variables and consisting in an extension to the nonequilibrium state of well-established equation of state (EOS) theories for penetrant−rubbery polymers mixtures, such as Sanchez−Lacombe theory (SL EOS),[24] perturbed chain statistical associating fluid theory (PC-SAFT EOS),[25] and perturbed hard-sphere chain theory (PHSCT),[26] to mention a few. This approach for the extension of these theories to nonequilibrium glassy polymers is referred to in the literature as nonequilibrium lattice fluid theory, NELF[23] (for to the specific case of the extension of SL EOS), or, more generally, as nonequilibrium thermodynamics for glassy polymers (NET-GP).[27] It introduces a modified expression for the chemical potentials in the polymer phase, based on the use of the density of the glassy polymer as an order parameter. A similar approach has been adopted by Panayiotou et al.[28]

However, it is worth noting that most of the available EOS theories for rubbery−penetrant systems at equilibrium (and, consequently, their extensions to nonequilibrium glassy polymers) fail to provide a good prediction of sorption behavior for systems involving specific interactions (e.g., hydrogen bonding). Notable exceptions are the approaches proposed for equilibrium systems endowed with long-range and short-range interactions[29–31] or, in particular, with H-bonding interactions.[32,33] However, none of these models have been extended yet to describe nonequilibrium glassy polymeric systems.

In fact, in the case at hand, a central role is played by H-bond interactions among water molecules and between water molecules and imide groups on the polymer backbone. In view of this limitation of the mentioned models and in the light of the spectroscopic results, we adopted a simpler approach to interpret sorption isotherms, which is based on the BET (Brunauer, Emmett, and Teller) multilayer adsorption theory[34,35] which enables the distinction among different penetrant "layers". In Scheme 1 it has been reported a schematic view of the possible

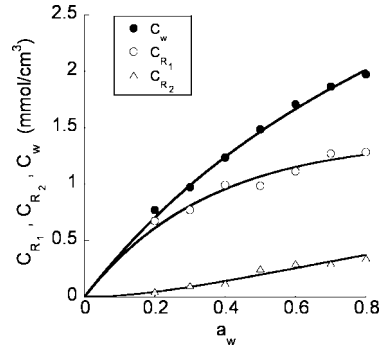

Figure 6. Concentration in PMDA-ODA, at sorption equilibrium, of total water (C_w), R_1 (C_{R_1}), and R_2 (C_{R_2}) species as a function of a_w. $T = 30$ °C.

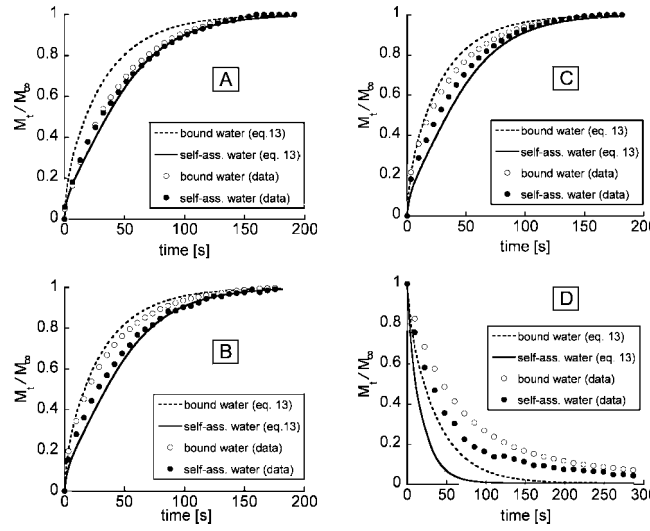

Figure 7. Sorption kinetics data and results of data fitting with eq 13 at $a_w = 0.2$ (A), $a_w = 0.4$ (B), and $a_w = 0.6$ (C). Desorption kinetics data and results of data fitting with eq 13 at $a_w = 0.4$ (D). Experimental results are reported as ratio of the amount of bound (○) and self-associated (●) water absorbed/desorbed at time t (M_t) and corresponding amounts absorbed/desorbed at equilibrium (M_∞). $T = 30$ °C.

interaction patterns of the various species involved. Sorbed water molecules are either interacting with imide groups ("bound water molecules", *b*) or are associated ("self-associated water molecules", *sa*) to water molecules, already bound to imide groups, forming water dimers. As already anticipated, we refer to single water molecules interacting with imide groups as R_1 species (their concentration being C_{R_1}) and to the bimolecular water aggregates as R_2 species (their concentration being C_{R_2}). There are straightforward relationships between C_{R_1} and C_{R_2} and C_b and C_{sa}, as detailed in the following equations (where with C_w is meant the total water concentration):

$$C_b = C_{R_1} + C_{R_2}$$

$$C_{sa} = C_{R_2}$$

$$C_w = C_b + C_{sa} = C_{R_1} + 2C_{R_2} \quad (6)$$

It is, then, a simple matter to estimate from spectroscopic measurements at water sorption equilibrium the equilibrium values of C_{R_1} and C_{R_2} at different water activities (see Figure 6). On the basis of this physical picture, the equilibrium data for C_{R_1} and C_{R_2} have been interpreted by using a modified multilayer BET adsorption equation,[35] where the sites of "adsorption" are the imide groups (i.e., R_0 in Scheme 1), and it has been imposed that the multilayer assembly is limited to a

maximum of two molecular layers because of the constraint imposed by the available free volume between adjacent backbones. As a consequence, we have the following equilibrium relationships:

$$a_1 P C_{R_0} = b_1 C_{R_1} \exp(-Q_1/RT)$$
$$a_2 P C_{R_1} = b_2 C_{R_2} \exp(-Q_2/RT) \quad (7)$$

where P is the pressure of the penetrant, a_1, a_2, b_1, and b_2 are constants, Q_1 and Q_2 are heats of interaction, and C_{R_0} is the concentration of "unoccupied" imide interaction sites. In the following we will refer to the total concentration of "accessible" imide sites as C_{R0MAX}, i.e., the sites available for interaction with water molecules. This value is expected to be lower than the actual total concentration of imide groups (C_{R0TOT}) originally present in the system. It follows that

$$C_{R_0} = C_{R_{0MAX}} - C_{R_1} - C_{R_2} \quad (8)$$

After some simple algebra, eqs 7 can be written as

$$\frac{C_{R_1}}{C_{R_{0MAX}}} = \frac{k_1 P}{1 + k_1 P(1 + P/k_2)}$$
$$\frac{C_{R_2}}{C_{R_{0MAX}}} = \frac{(k_1/k_2)P^2}{1 + k_1 P(1 + P/k_2)} \quad (9)$$

where k_1 and k_2 are temperature-dependent dimensional parameters (respectively expressed in [pressure units]$^{-1}$ and [pressure units]).

By defining $a = P/P_0$, where P_0 is the vapor pressure of water at the temperature of interest, eqs 9 can be recast as

$$C_{R_1} = \frac{K_1 C_{R_{0MAX}} a}{1 + K_1 a(1 + K_2 a)}$$
$$C_{R_2} = \frac{K_1 K_2 C_{R_{0MAX}} a^2}{1 + K_1 a(1 + K_2 a)} \quad (10)$$

where $K_1 = k_1 P_0$ and $K_2 = P_0/k_2$ are dimensionless parameters. Consequently

$$C_w = C_{R_1} + 2C_{R_2} = \frac{K_1 C_{R_{0MAX}} a(1 + 2K_2 a)}{1 + K_1 a(1 + K_2 a)} \quad (11)$$

The previous equations imply that the equilibrium values of C_{R_1} and C_{R_2} are related to each other by a nonlinear relationship (in the following simply referred to as $C_{R_1} = f(C_{R_2})$). Data for C_{R_1} and C_{R_2} as a function of relative humidity, a_w, have been fitted using eqs 10. The following values of K_1, K_2, and C_{R0MAX} have been obtained after performing a concurrent best fitting of both data sets (see Figure 6): $K_1 = 1.5 \pm 0.05$, $K_2 = 0.37 \pm 0.02$, and $C_{R_{0MAX}} = 2.70 \pm 0.15$ mmol/cm^3.

The results of this experimental analysis reveal that, as expected, the concentration of "available" imide sites, i.e. C_{R0MAX}, is 2.7 mmol/cm^3, which corresponds to only 35% of the total number of imide groups originally present in the system, i.e., C_{R0TOT}, which amounts to 7.7 mmol/cm^3. Therefore, a conspicuous fraction of imide groups is to be considered inert toward water molecules, either because of steric constraints or because these groups are already involved in intermolecular charge transfer interactions which drastically reduce their tendency to act as proton acceptors.

Sorption/Desorption Kinetics. On the basis of the spectroscopic analysis, it can be inferred that mass transport of water in PMDA-ODA involves R_1 and R_2 species. Furthermore, in view of the higher interaction energy between two water molecules as compared to the case of water molecules interacting with imide groups, it is expected that the hypothesized water

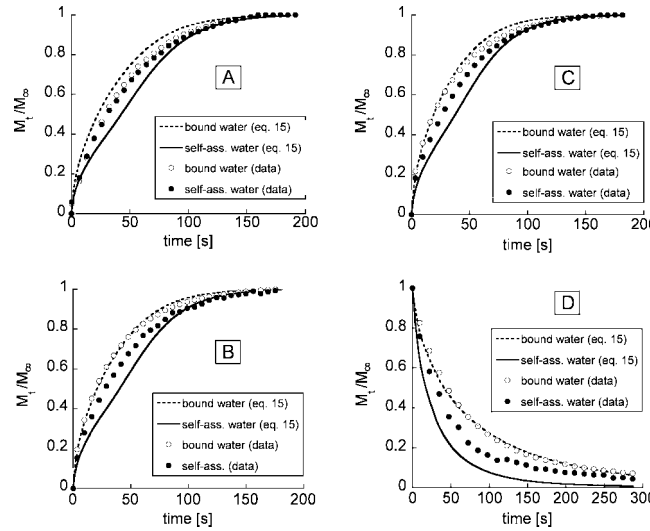

Figure 8. Sorption kinetics data and results of data fitting with eq 15 at $a_w = 0.2$ (A), $a_w = 0.4$ (B), and $a_w = 0.6$ (C). Desorption kinetics data and results of data fitting with eq 13 at $a_w = 0.4$ (D). Experimental results are reported as ratio of the amount of bound (○) and self-associated (●) water absorbed/desorbed at time t (M_t) and corresponding amounts absorbed/desorbed at equilibrium (M_∞). $T = 30$ °C.

dimers move as a whole. Thus, the whole process is likely to occur by successive jumps of R_1 and R_2 species.

Moreover, the spectroscopic evidence suggests that an instantaneous nonlinear equilibrium establishes locally between R_1 and R_2 species. As a consequence, water transport can be assumed to be ruled by the following differential mass balance, which is valid in the limit of small penetrant concentration and under the assumption that the flux of each species does not depend on the concentration gradient of the other:

$$\frac{\partial C_w}{\partial t} = \frac{\partial}{\partial x}\left(D_1 \frac{\partial C_{R_1}}{\partial x}\right) + 2\frac{\partial}{\partial x}\left(D_2 \frac{\partial C_{R_2}}{\partial x}\right) \quad (12)$$

where $C_{R_2} = f(C_{R_1})$, $C_w = C_{R_1} + 2C_{R_2} = C_{R_1} + 2f(C_{R_1})$, and D_1 and D_2 are the mutual diffusivities of each species and can be dependent on concentration.

By simple algebra and assuming constant diffusivities, we obtain the following differential equation for C_{R_1}:

$$[1 + 2f'(C_{R_1})]\frac{\partial C_{R_1}}{\partial t} = 2D_2 f''(C_{R_1})\left(\frac{\partial C_{R_1}}{\partial x}\right)^2 + [D_1 + 2D_2 f'(C_{R_1})]\frac{\partial^2 C_{R_1}}{\partial x^2} \quad (13)$$

where

$$f'(C_{R_1}) = \frac{\partial f}{\partial C_{R_1}}; \quad f''(C_{R_1}) = \frac{\partial^2 f}{\partial C_{R_1}^2}$$

On the basis of this approach, and in view of the nonlinear nature of the equilibrium relationship, it is expected that, independently of the relative values of the diffusivities, the normalized sorption kinetics of R_1 species is faster than that of R_2 species. This behavior is reversed in the case of desorption kinetics (i.e., desorption is faster in the case of R_2 species). It is worth noting that, if the local instantaneous equilibrium relationship were linear, the sorption kinetics of both species would be coincident, independently of the relative values of diffusivities.

The method of lines[36] has been adopted to numerically solve eq 13. The numerical solution has been used to interpret

sorption−desorption kinetics as evaluated spectroscopically after having used eqs 6 to convert C_{R_1} and C_{R_2} in terms of C_b and C_{sa}. Sorption−desorption data fitting has been performed concurrently on all available data. The estimated values of D_1 and D_2 are respectively $1.75 \times 10^{-12} \pm 1 \times 10^{-13}$ cm^2/s and $1.55 \times 10^{-12} \pm 1 \times 10^{-13}$ cm^2/s. In Figure 7A−D model predictions are compared to experimental data for sorption at $a_w = 0.2$, 0.4, and 0.6 and for desorption at $a_w = 0.4$, reported as ratio of the amount of bound water and self-associated water absorbed/desorbed at time t (M_t) and corresponding amounts absorbed/desorbed at equilibrium (M_∞), as a function of time. It is evident that the experimental features are qualitatively captured by the model, with particular reference to the observed relative evolution rate of bound and self-associated water concentration during sorption and desorption. The quantitative agreement, however, appears to be unsatisfactory, especially for desorption kinetics. This is likely due to the assumption of independence of diffusivities on water concentration, which is generally not observed for water transport in glassy polymers. In the present case, the faster kinetics observed in sorption experiments as compared to desorption, points to an increase of diffusivity with penetrant concentration. Accordingly, to gain a better quantitative simulation of the physical behavior, it has been assumed that both diffusion coefficients are actually dependent on total water concentration, i.e.

$$D_i = D_i^0 \exp[kC_w] = D_i^0 \exp[k(C_{R_1} + 2f(C_{R_1}))] \qquad (14)$$

Accordingly, eq 13 becomes

$$[1 + 2f'(C_{R_1})]\frac{\partial C_{R_1}}{\partial t} = \{D_1 k[1 + 2f'(C_{R_1})] + 2D_2 f''(C_{R_1}) + 2D_2 k[1 + 2f'(C_{R_1})]f'(C_{R_1})\}\left(\frac{\partial C_{R_1}}{\partial x}\right)^2 + [D_1 + 2D_2 f'(C_{R_1})]\frac{\partial^2 C_{R_1}}{\partial x^2} \qquad (15)$$

Use of eq 15 to fit spectroscopic data actually resulted in a somewhat better global quantitative agreement between model prediction and experimental kinetics data (see Figure 8A−D). Concurrent best fitting of all sorption/desorption data supplied the following values for the model parameters: $D_{0,1} = 4.5 \times 10^{-13} \pm 1 \times 10^{-13}$ cm^2/s; $D_{0,2} = 1.7 \times 10^{-13} \pm 1 \times 10^{-13}$ cm^2/s; $k = 1.55 \pm 3 \times 10^{-2}$ cm^3/mmol. As expected, in view of their higher volume, R_2 species display a lower diffusivity.

Conclusion

In the present contribution a model has been developed to describe water transport in a PMDA-ODA polyimide at 30 °C and at several relative humidity levels.

The model is based on the physical picture of an instantaneous nonlinear equilibrium between two distinct water species evolving with different kinetics, which is suggested by the results of a time-resolved in situ FTIR analysis of sorption/desorption processes. The proposed model is able to describe effectively the behavior of the system with respect to both the equilibrium and the dynamic evolution, supplying also a semiquantitative interpretation of the observed phenomena.

In particular, sorption thermodynamics has been successfully interpreted by using a two-layer BET isotherm, where the adsorption sites are represented by the imide groups of the polymer backbone and the penetrant−site interaction occurs through H-bonding, while sorption/desorption kinetics has been modeled by assuming a different mobility for the water species involved, gaining a better quantitative agreement with the experimental results when dependence of diffusivities on total water concentration was introduced.

References and Notes

(1) Gosh, M. K., Mittal, K. L., Eds.; *Polyimides: Fundamentals and Applications*; Marcel Dekker: New York, 1996.
(2) Bessonov, M. I.; Zubkov, V. A. *Polyamic Acids and Polyimides: Synthesis, Transformation and Structure*; CRC Press: Boca Raton, FL, 1993.
(3) Thompson, L. F., Willson, C. G., Tagawa, S., Eds.; *Polymers for Microelectronics: Resists and Dielectrics*; ACS Symposium Series 537; American Chemical Society: Washington, DC, 1994.
(4) Feger, C.; Khojasteh, M. M.; Htoo, M. S. *Advances in Polyimide Science and Technology*; Technomic: Lancaster, PA, 1993.
(5) Roberson, L. M. *J. Membr. Sci.* **1991**, *62*, 165.
(6) Stern, S. A. *J. Membr. Sci.* **1994**, *94*, 1.
(7) Kim, T. H.; Koros, W. J.; Husk, G. R.; O'Brien, K. C. *J. Membr. Sci.* **1988**, *37*, 45.
(8) Coleman, M. R.; Koros, W. J. *J. Membr. Sci.* **1990**, *50*, 285.
(9) Thompson, L. F., Wilson, C. G., Tagawa, S., Eds.; *Polymers for Microelectronics: Resists and Dielectrics*; ACS Symposium Series 537; American Chemical Society: Washington, DC, 1994.
(10) Seo, J.; Han, H. *J. Appl. Polym. Sci.* **2001**, *82*, 731.
(11) Lim, B. S.; Nowick, A. S.; Lee, K.; Viehbeck, A. *J. Polym. Sci., Part B: Polym. Phys. Ed.* **1993**, *31*, 545.
(12) Merdas, I.; Thominette, F.; Verdu, J. *J. Appl. Polym. Sci.* **2000**, *77*, 1439.
(13) Punsalan, D.; Koros, W. J. *J. Appl. Polym. Sci.* **2005**, *96*, 1115.
(14) Musto, P.; Ragosta, G.; Mensitieri, G.; Lavorgna, M. *Macromolecules* **2007**, *40*, 9614.
(15) Cotugno, S.; Larobina, D.; Mensitieri, G.; Musto, P.; Ragosta, G. *Polymer* **2000**, *42*, 6431.
(16) Mensitieri, G.; Cotugno, S.; Musto, P.; Ragosta, G.; Nicolais, L. Transport of Water in High T_g Polymers: A Comparison Between Interacting and Non-Interacting Systems. In *Polyimides and Other High Temperature Polymers: Synthesis, Characterization and Applications*; Mittal, K. L., Ed.; VSP Publ.: The Netherlands, 2003; Vol. 2.
(17) Noda, I.; Ozaki, Y. *Two-Dimensional Correlation Spectroscopy*; Wiley: Chichester, UK, 2004.
(18) Noda, I. *Appl. Spectrosc.* **2000**, *54*, 994.
(19) Skrovanek, D. J.; Howe, S. E.; Painter, P. C.; Coleman, M. M. *Macromolecules* **1985**, *18*, 1676.
(20) Skrovanek, D. J.; Painter, P. C.; Coleman, M. M. *Macromolecules* **1986**, *19*, 699.
(21) Pimentel, G. C.; McClellan, A. L. *The Hydrogen Bond*; W.H. Freeman and Co.: San Francisco, 1960.
(22) Murthy, A. S. N.; Rao, C. N. R. *Appl. Spectrosc. Rev.* **1968**, *2*, 69.
(23) Doghieri, F.; Sarti, G. C. *Macromolecules* **1996**, *29*, 7885.
(24) Sanchez, I. C.; Lacombe, R. H. *Macromolecules* **1978**, *11*, 1145.
(25) Gross, J.; Sadowsky, G. *Ind. Eng. Chem. Res.* **2001**, *40*, 1244.
(26) Song, Y.; Lambert, S. M.; Prausnitz, J. M. *Ind. Eng. Chem. Res.* **1994**, *33*, 1047.
(27) de Angelis, M. G.; Doghieri, F.; Sarti, G. C.; Freeman, B. D. *Desalination* **2006**, *193*, 82.
(28) Boudouris, D.; Panayiotou, C. *Macromolecules* **1998**, *31*, 7915.
(29) Gross, J. *AIChE J.* **2005**, *51*, 2556.
(30) Gross, J.; Vrabec, J. *AIChE J.* **2006**, *52*, 1194.
(31) Kleiner, M.; Gross, J. *AIChE J.* **2006**, *52*, 1951.
(32) Panayiotou, C. *J. Chem. Thermodyn.* **2003**, *35*, 349.
(33) Panayiotou, C.; Tsivintzelis, I.; Economou, I. G. *Ind. Eng. Chem. Res.* **2007**, *46*, 2628.
(34) Brunauer, S.; Emmett, P. H.; Teller, E. *J. Am. Chem. Soc.* **1938**, *60*, 309.
(35) Adamson, A. W. *Physical Chemistry of Surfaces*, 5th ed.; John Wiley & Sons: New York, 1990; Chapter 16.
(36) Schiesser, W. E. *The Numerical Method of Lines*; Academic Press: San Diego, CA, 1991.

MA8004422